

Charged particle distributions and nuclear modification at high rapidities in d+Au collisions at $\sqrt{s_{NN}} = 200$ GeV

B.I. Abelev,⁹ M.M. Aggarwal,³⁰ Z. Ahammed,⁴⁵ B.D. Anderson,²⁰ D. Arkhipkin,¹³ G.S. Averichev,¹² Y. Bai,²⁸ J. Balewski,¹⁷ O. Barannikova,⁹ L.S. Barnby,² J. Baudot,¹⁸ S. Baumgart,⁵⁰ V.V. Belaga,¹² A. Bellingeri-Laurikainen,⁴⁰ R. Bellwied,⁴⁸ F. Benedosso,²⁸ R.R. Betts,⁹ S. Bhardwaj,³⁵ A. Bhasin,¹⁹ A.K. Bhati,³⁰ H. Bichsel,⁴⁷ J. Bielcik,⁵⁰ J. Bielcikova,⁵⁰ L.C. Bland,³ S-L. Blyth,²² M. Bombara,² B.E. Bonner,³⁶ M. Botje,²⁸ J. Bouchet,⁴⁰ A.V. Brandin,²⁶ A. Bravar,³ T.P. Burton,² M. Bystersky,¹¹ R.V. Cadman,¹ X.Z. Cai,³⁹ H. Caines,⁵⁰ M. Calderón de la Barca Sánchez,⁶ J. Callner,⁹ O. Catu,⁵⁰ D. Cebra,⁶ Z. Chajecski,²⁹ P. Chaloupka,¹¹ S. Chattopadhyay,⁴⁵ H.F. Chen,³⁸ J.H. Chen,³⁹ J.Y. Chen,⁴⁹ J. Cheng,⁴³ M. Cherney,¹⁰ A. Chikhanian,⁵⁰ W. Christie,³ S.U. Chung,³ J.P. Coffin,¹⁸ T.M. Cormier,⁴⁸ M.R. Cosentino,³⁷ J.G. Cramer,⁴⁷ H.J. Crawford,⁵ D. Das,⁴⁵ S. Dash,¹⁵ M. Daugherty,⁴² M.M. de Moura,³⁷ T.G. Dedovich,¹² M. DePhillips,³ A.A. Derevschikov,³² L. Didenko,³ T. Dietel,¹⁴ P. Djawotho,¹⁷ S.M. Dogra,¹⁹ X. Dong,²² J.L. Drachenberg,⁴¹ J.E. Draper,⁶ F. Du,⁵⁰ V.B. Dunin,¹² J.C. Dunlop,³ M.R. Dutta Mazumdar,⁴⁵ V. Eckardt,²⁴ W.R. Edwards,²² L.G. Efimov,¹² V. Emelianov,²⁶ J. Engelage,⁵ G. Eppley,³⁶ B. Erazmus,⁴⁰ M. Estienne,¹⁸ P. Fachini,³ R. Fatemi,²³ J. Fedorisin,¹² A. Feng,⁴⁹ P. Filip,¹³ E. Finch,⁵⁰ V. Fine,³ Y. Fisyak,³ J. Fu,⁴⁹ C.A. Gagliardi,⁴¹ L. Gaillard,² M.S. Ganti,⁴⁵ E. Garcia-Solis,⁹ V. Ghazikhanian,⁷ P. Ghosh,⁴⁵ Y.G. Gorbunov,¹⁰ H. Gos,⁴⁶ O. Grebenyuk,²⁸ D. Grosnick,⁴⁴ S.M. Guertin,⁷ K.S.F.F. Guimaraes,³⁷ N. Gupta,¹⁹ B. Haag,⁶ T.J. Hallman,³ A. Hamed,⁴¹ J.W. Harris,⁵⁰ W. He,¹⁷ M. Heinz,⁵⁰ T.W. Henry,⁴¹ S. Heppelmann,³¹ B. Hippolyte,¹⁸ A. Hirsch,³³ E. Hjort,²² A.M. Hoffman,²³ G.W. Hoffmann,⁴² D. Hofman,⁹ R. Hollis,⁹ M.J. Horner,²² H.Z. Huang,⁷ E.W. Hughes,⁴ T.J. Humanic,²⁹ G. Igo,⁷ A. Iordanova,⁹ P. Jacobs,²² W.W. Jacobs,¹⁷ P. Jakl,¹¹ F. Jia,²¹ P.G. Jones,² E.G. Judd,⁵ S. Kabana,⁴⁰ K. Kang,⁴³ J. Kapitan,¹¹ M. Kaplan,⁸ D. Keane,²⁰ A. Kechechyan,¹² D. Kettler,⁴⁷ V.Yu. Khodyrev,³² B.C. Kim,³⁴ J. Kiryluk,²² A. Kisiel,⁴⁶ E.M. Kislov,¹² S.R. Klein,²² A.G. Knospe,⁵⁰ A. Kocoloski,²³ D.D. Koetke,⁴⁴ T. Kollegger,¹⁴ M. Kopytine,²⁰ L. Kotchenda,²⁶ V. Kouchpil,¹¹ K.L. Kowalik,²² P. Kravtsov,²⁶ V.I. Kravtsov,³² K. Krueger,¹ C. Kuhn,¹⁸ A.I. Kulikov,¹² A. Kumar,³⁰ P. Kurnadi,⁷ A.A. Kuznetsov,¹² M.A.C. Lamont,⁵⁰ J.M. Landgraf,³ S. Lange,¹⁴ S. LaPointe,⁴⁸ F. Laue,³ J. Lauret,³ A. Lebedev,³ R. Lednický,¹³ C-H. Lee,³⁴ S. Lehocka,¹² M.J. LeVine,³ C. Li,³⁸ Q. Li,⁴⁸ Y. Li,⁴³ G. Lin,⁵⁰ X. Lin,⁴⁹ S.J. Lindenbaum,²⁷ M.A. Lisa,²⁹ F. Liu,⁴⁹ H. Liu,³⁸ J. Liu,³⁶ L. Liu,⁴⁹ T. Ljubicic,³ W.J. Llope,³⁶ R.S. Longacre,³ W.A. Love,³ Y. Lu,⁴⁹ T. Ludlam,³ D. Lynn,³ G.L. Ma,³⁹ J.G. Ma,⁷ Y.G. Ma,³⁹ D. Magestro,²⁹ D.P. Mahapatra,¹⁵ R. Majka,⁵⁰ L.K. Mangotra,¹⁹ R. Manweiler,⁴⁴ S. Margetis,²⁰ C. Markert,⁴² L. Martin,⁴⁰ H.S. Matis,²² Yu.A. Matulenko,³² C.J. McClain,¹ T.S. McShane,¹⁰ Yu. Melnick,³² A. Meschanin,³² J. Millane,²³ M.L. Miller,²³ N.G. Minaev,³² S. Mioduszewski,⁴¹ C. Mironov,²⁰ A. Mischke,²⁸ J. Mitchell,³⁶ B. Mohanty,²² D.A. Morozov,³² M.G. Munhoz,³⁷ B.K. Nandi,¹⁶ C. Nattrass,⁵⁰ T.K. Nayak,⁴⁵ J.M. Nelson,² N.S. Nepali,²⁰ P.K. Netrakanti,³³ L.V. Nogach,³² S.B. Nurushev,³² G. Odyniec,²² A. Ogawa,³ V. Okorokov,²⁶ M. Oldenburg,²² D. Olson,²² M. Pachr,¹¹ S.K. Pal,⁴⁵ Y. Panebratsev,¹² A.I. Pavlinov,⁴⁸ T. Pawlak,⁴⁶ T. Peitzmann,²⁸ V. Perevoztchikov,³ C. Perkins,⁵ W. Peryt,⁴⁶ S.C. Phatak,¹⁵ M. Planinic,⁵¹ J. Pluta,⁴⁶ N. Poljak,⁵¹ N. Porile,³³ A.M. Poskanzer,²² M. Potekhin,³ E. Potrebenikova,¹² B.V.K.S. Potukuchi,¹⁹ D. Prindle,⁴⁷ C. Pruneau,⁴⁸ J. Putschke,²² I.A. Qattan,¹⁷ R. Raniwala,³⁵ S. Raniwala,³⁵ R.L. Ray,⁴² D. Relyea,⁴ A. Ridiger,²⁶ H.G. Ritter,²² J.B. Roberts,³⁶ O.V. Rogachevskiy,¹² J.L. Romero,⁶ A. Rose,²² C. Roy,⁴⁰ L. Ruan,²² M.J. Russcher,²⁸ R. Sahoo,¹⁵ I. Sakrejda,²² T. Sakuma,²³ S. Salur,⁵⁰ J. Sandweiss,⁵⁰ M. Sarsour,⁴¹ P.S. Sazhin,¹² J. Schambach,⁴² R.P. Scharenberg,³³ N. Schmitz,²⁴ J. Seger,¹⁰ I. Selyuzhenkov,⁴⁸ P. Seyboth,²⁴ A. Shabetai,¹⁸ E. Shahaliev,¹² M. Shao,³⁸ M. Sharma,³⁰ W.Q. Shen,³⁹ S.S. Shimanskiy,¹² E.P. Sichtermann,²² F. Simon,²³ R.N. Singaraju,⁴⁵ N. Smirnov,⁵⁰ R. Snellings,²⁸ P. Sorensen,³ J. Sowinski,¹⁷ J. Speltz,¹⁸ H.M. Spinka,¹ B. Srivastava,³³ A. Stadnik,¹² T.D.S. Stanislaus,⁴⁴ D. Staszak,⁷ R. Stock,¹⁴ M. Strikhanov,²⁶ B. Stringfellow,³³ A.A.P. Suaide,³⁷ M.C. Suarez,⁹ N.L. Subba,²⁰ M. Sumbera,¹¹ X.M. Sun,²² Z. Sun,²¹ B. Surrow,²³ T.J.M. Symons,²² A. Szanto de Toledo,³⁷ J. Takahashi,³⁷ A.H. Tang,³ T. Tarnowsky,³³ J.H. Thomas,²² A.R. Timmins,² S. Timoshenko,²⁶ M. Tokarev,¹² T.A. Trainor,⁴⁷ S. Trentalange,⁷ R.E. Tribble,⁴¹ O.D. Tsai,⁷ J. Ulery,³³ T. Ullrich,³ D.G. Underwood,¹ G. Van Buren,³ N. van der Kolk,²⁸ M. van Leeuwen,²² A.M. Vander Molen,²⁵ R. Varma,¹⁶ I.M. Vasilevski,¹³ A.N. Vasiliev,³² R. Vernet,¹⁸ S.E. Vigdor,¹⁷ Y.P. Viyogi,¹⁵ S. Vokal,¹² S.A. Voloshin,⁴⁸ W.T. Waggoner,¹⁰ F. Wang,³³ G. Wang,⁷ J.S. Wang,²¹ X.L. Wang,³⁸ Y. Wang,⁴³ J.W. Watson,²⁰ J.C. Webb,⁴⁴ G.D. Westfall,²⁵ A. Wetzler,²² C. Whitten Jr.,⁷ H. Wieman,²² S.W. Wissink,¹⁷ R. Witt,⁵⁰ J. Wu,³⁸ Y. Wu,⁴⁹ N. Xu,²² Q.H. Xu,²² Z. Xu,³ P. Yepes,³⁶ I-K. Yoo,³⁴ Q. Yue,⁴³ V.I. Yurevich,¹² W. Zhan,²¹ H. Zhang,³ W.M. Zhang,²⁰ Y. Zhang,³⁸ Z.P. Zhang,³⁸ Y. Zhao,³⁸ C. Zhong,³⁹ J. Zhou,³⁶ R. Zoukarneev,¹³ Y. Zoukarneeva,¹³ A.N. Zubarev,¹² and J.X. Zuo³⁹

(STAR Collaboration)

- ¹Argonne National Laboratory, Argonne, Illinois 60439
²University of Birmingham, Birmingham, United Kingdom
³Brookhaven National Laboratory, Upton, New York 11973
⁴California Institute of Technology, Pasadena, California 91125
⁵University of California, Berkeley, California 94720
⁶University of California, Davis, California 95616
⁷University of California, Los Angeles, California 90095
⁸Carnegie Mellon University, Pittsburgh, Pennsylvania 15213
⁹University of Illinois, Chicago
¹⁰Creighton University, Omaha, Nebraska 68178
¹¹Nuclear Physics Institute AS CR, 250 68 Řež/Prague, Czech Republic
¹²Laboratory for High Energy (JINR), Dubna, Russia
¹³Particle Physics Laboratory (JINR), Dubna, Russia
¹⁴University of Frankfurt, Frankfurt, Germany
¹⁵Institute of Physics, Bhubaneswar 751005, India
¹⁶Indian Institute of Technology, Mumbai, India
¹⁷Indiana University, Bloomington, Indiana 47408
¹⁸Institut de Recherches Subatomiques, Strasbourg, France
¹⁹University of Jammu, Jammu 180001, India
²⁰Kent State University, Kent, Ohio 44242
²¹Institute of Modern Physics, Lanzhou, China
²²Lawrence Berkeley National Laboratory, Berkeley, California 94720
²³Massachusetts Institute of Technology, Cambridge, MA 02139-4307
²⁴Max-Planck-Institut für Physik, Munich, Germany
²⁵Michigan State University, East Lansing, Michigan 48824
²⁶Moscow Engineering Physics Institute, Moscow Russia
²⁷City College of New York, New York City, New York 10031
²⁸NIKHEF and Utrecht University, Amsterdam, The Netherlands
²⁹Ohio State University, Columbus, Ohio 43210
³⁰Panjab University, Chandigarh 160014, India
³¹Pennsylvania State University, University Park, Pennsylvania 16802
³²Institute of High Energy Physics, Protvino, Russia
³³Purdue University, West Lafayette, Indiana 47907
³⁴Pusan National University, Pusan, Republic of Korea
³⁵University of Rajasthan, Jaipur 302004, India
³⁶Rice University, Houston, Texas 77251
³⁷Universidade de Sao Paulo, Sao Paulo, Brazil
³⁸University of Science & Technology of China, Hefei 230026, China
³⁹Shanghai Institute of Applied Physics, Shanghai 201800, China
⁴⁰SUBATECH, Nantes, France
⁴¹Texas A&M University, College Station, Texas 77843
⁴²University of Texas, Austin, Texas 78712
⁴³Tsinghua University, Beijing 100084, China
⁴⁴Valparaiso University, Valparaiso, Indiana 46383
⁴⁵Variable Energy Cyclotron Centre, Kolkata 700064, India
⁴⁶Warsaw University of Technology, Warsaw, Poland
⁴⁷University of Washington, Seattle, Washington 98195
⁴⁸Wayne State University, Detroit, Michigan 48201
⁴⁹Institute of Particle Physics, CCNU (HZNU), Wuhan 430079, China
⁵⁰Yale University, New Haven, Connecticut 06520
⁵¹University of Zagreb, Zagreb, HR-10002, Croatia

The measurements of the centrality dependence of $dN/d\eta$ and transverse momentum spectra from mid- to forward rapidity in d+Au collisions at $\sqrt{s_{NN}} = 200$ GeV are reported. They provide a sensitive tool for understanding the dynamics of multi-particle production in the high parton-density regime. In particular, we observe strong suppression of the nuclear modification factor R_{CP} at forward rapidities (d-side, $\eta = 3.1$) and enhancement at backward rapidity ($\eta = -3.1$). An empirical scaling is obtained for multiplicity and R_{CP} when a shift of the center-of-mass in the asymmetric d+Au collisions with respect to the nucleon-nucleon system is applied.

PACS numbers: 25.75.-q, 25.75.Dw, 13.85.-t

I. INTRODUCTION

The d+Au collisions at the Relativistic Heavy Ion Collider (RHIC) provide an important control environment

compared to Au+Au collisions. Measurements of the nu-

clear modification factor and back-to-back correlations at mid-rapidity in d+Au collisions suggest that the suppression of particles with high transverse momentum and the disappearance of back-to-back correlations, seen in Au+Au collisions [1], are due to final-state interactions with the hot, dense medium produced in such collisions, rather than initial-state effects on the Au nucleus [2]. The observed enhancement of the nuclear modification factor in the region of transverse momentum (p_t) of 2 GeV/c at mid-rapidity in d+Au collisions [3, 4, 5, 6], referred to as the ‘‘Cronin effect’’ [7], can be described within a pQCD framework incorporating initial multiple parton scattering and nuclear shadowing [8, 9]. Saturation effects (mostly described as the formation of Color Glass Condensate (CGC) [10]) are expected to be more pronounced at large rapidity (y) or pseudorapidity (η) close to the deuteron beam, where the small- x components of the Au nucleus wave function can be probed. Recent results reported by the BRAHMS collaboration [11], where a suppression of the nuclear modification factor at forward rapidities is visible, are in qualitative agreement with predictions within the framework of gluon saturation in the CGC [12]. These results indicate a possible dramatic evolution of gluon saturation from mid- to forward rapidity at RHIC. However, it should be noted that these results can be reasonably described by pQCD models [8, 9] and in the framework of final-state parton recombination [13]. On the other hand, as the rapidity of the probe decreases (and at the same time, x increases), the multiple-scattering contribution to the Cronin effect should decrease. The first results from the PHENIX collaboration [14] show an opposite behaviour which cannot be explained by current model calculations [15].

In this paper the pseudorapidity and centrality dependence of the nuclear modification factor R_{CP} will be discussed in connection with the asymmetry in particle production in d+Au collisions at $\sqrt{s_{NN}}=200$ GeV.

II. EXPERIMENTAL SETUP

The STAR experiment [16] at RHIC measures charged hadrons over a wide range of pseudorapidity and transverse momentum. The main detector is a large Time Projection Chamber (TPC) [17] which allows particle identification via dE/dx within the range of $|\eta| < 1$. Charged particle detection in the forward directions is achieved with the two azimuthally symmetric Forward TPC (FTPCs) [18] which extend the pseudorapidity coverage of STAR to the region $2.5 < |\eta| < 4$. The FTPCs which utilize a radial drift field perpendicular to the magnetic field, achieve a two-track resolution of 2 – 2.5 mm (an order of magnitude better than a TPC using a constant drift field). This allows track reconstruction in the larger rapidity region where track densities are high. In d+Au collisions at a center-of-mass energy of $\sqrt{s_{NN}}=200$ GeV a track finding efficiency in the FTPCs of about 90% was reached, independent of centrality, η and p_t in the phase

space region of $3 < \eta < 3.5$ and $0.1 < p_t < 3$ GeV/c used for this analysis. The momentum resolution in the FTPCs is also independent of centrality, but shows a strong dependence on η and p_t . For $\eta \approx 3.1$, the relative momentum resolution degrades approximately linearly from 10% to 25% – 30% in the region of $0.1 < p_t < 3$ GeV/c and the pseudorapidity resolution is better than 0.02 units in η . Background and secondary decay products corrections were estimated using HIJING simulations [19]. The main systematic error quoted in this analysis (if not otherwise mentioned) is caused by the momentum resolution of the FTPCs. This affected mainly the vertex DCA (distance of closest approach) requirement used to select primary charged hadrons in the FTPCs. An estimate of the main systematic error was done by varying the DCA by ± 0.5 cm. A detailed description of the various calibration steps, further corrections and data quality can be found in [20].

III. MEASUREMENTS

A. Mean transverse momentum

To quantify the influence of momentum resolution on the transverse momentum spectra simulated charged pions were embedded in real d+Au events, adding up to 5% of the total event multiplicity in the FTPCs. Initially flat input distributions were weighted according to the measured transverse momentum distributions as function of centrality and transverse momentum [20]. Background and secondary decay products corrections were estimated using HIJING simulations [19, 20]. The transverse momentum distributions corrected for momentum resolution, background and secondary decay products measured in the East-FTPC (Au-side; $\eta \approx -3.1$) and West-FTPC (d-side; $\eta \approx 3.1$) are shown in Fig. 1a for different centrality classes. Fig. 1b shows the mean transverse momentum $\langle p_t \rangle$ obtained from a power-law fit to the measured p_t spectra in the region of $0.1 < p_t < 1$ GeV/c as a function of the number N_{part} of participant nucleons. In contrast to the ‘‘naive’’ picture in which the partons from the d-nucleus experience multiple collisions while traversing the Au-nucleus, and therefore acquire an enhancement of $\langle p_t \rangle$ on the d-side of the collision [15], a slight increase of $\langle p_t \rangle$ with centrality is visible on the Au-side, whereas on the d-side virtually no centrality dependence of $\langle p_t \rangle$ is present.

B. R_{CP} in the forward directions

Another variable of interest is the ratio of central to peripheral inclusive d+Au spectra

$$R_{CP}(p_t) = \frac{(d^2 N / dp_t d\eta / \langle N_{bin} \rangle) |_{central}}{(d^2 N / dp_t d\eta / \langle N_{bin} \rangle) |_{periph}}, \quad (1)$$

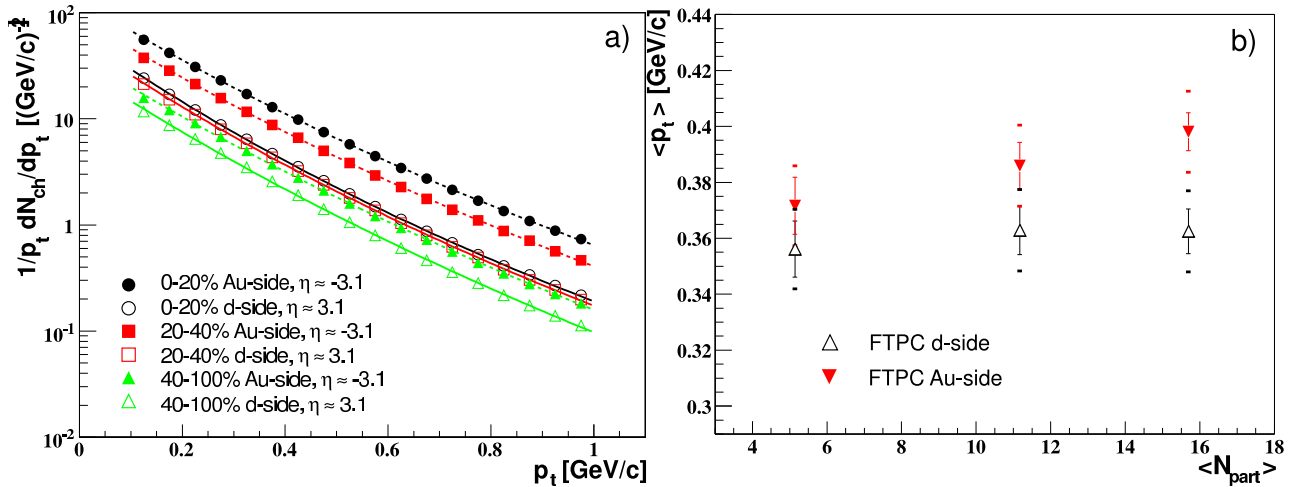


FIG. 1: (Color online) a) Charged hadron transverse momentum distributions at $|\eta| \approx 3.1$ for 0-20%, 20-40% and 40-100% central d+Au events. Closed triangles refer to measurements on the Au-side ($\eta \approx -3.1$) and open triangles to the d-side ($\eta \approx 3.1$). b) $\langle p_t \rangle$ extracted from fitting the transverse momentum spectra with a power law function at $|\eta| \approx 3.1$ as a function of N_{part} . The closed triangles are measurements on the Au-side and the open triangles on the d-side of a d+Au collision. Statistical (lines) and systematical (bars) are shown separately (for details see text).

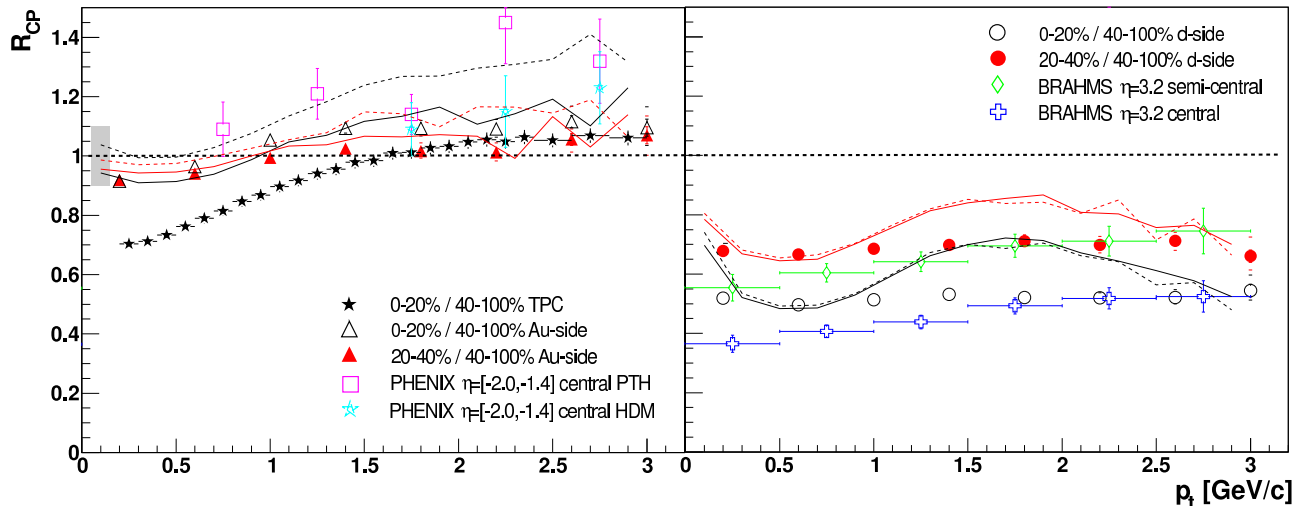


FIG. 2: (Color online) R_{CP} at $\eta \approx -3.1$ (Au-side; triangles) and at $\eta \approx 3.1$ (d-side; circles) for 20% and 20-40% central d+Au events. The grey band represents the estimate of the systematic error [20]. Midrapidity charged hadron R_{CP} (0-20%) ($|\eta| < 0.5$) is shown as stars [21]. Measurements from BRAHMS at $\eta \approx 3.2$ on the d-side [11] and from PHENIX in the region of $-2 < \eta < -1.4$ on the Au-side [14] are also overlaid. The solid lines represent HIJING simulations [19] without shadowing, the dashed lines with shadowing.

where $d^2N/dp_t d\eta$ is the differential yield per event and $\langle N_{bin} \rangle$ the mean number of binary collisions for the corresponding centrality class, calculated using a Monte Carlo Glauber model [3] (see Table I). For the R_{CP} measurements the transverse momentum range could be expanded to 3 GeV/c (instead of 1 GeV/c for the transverse momentum measurements in section III A) due to the centrality independence of the momentum resolution. Therefore, the effect of momentum resolution on the transverse momentum spectra cancels out in the R_{CP} ratio.

Centrality class	N_{part}	N_{bin}
0-20%	15.69 ± 1.19	15.07 ± 1.29
20-40%	11.17 ± 1.11	10.61 ± 0.80
40-100%	5.14 ± 0.44	4.21 ± 0.49
0-100%	8.31 ± 0.37	7.51 ± 0.39

TABLE I: N_{part} and N_{bin} for various centrality classes.

Comparing forward to backward rapidities, it can be seen in Fig. 2 that R_{CP} is increasing with p_t for $p_t < 3$ GeV/c on the Au-side. Also R_{CP} is larger on the Au-side,

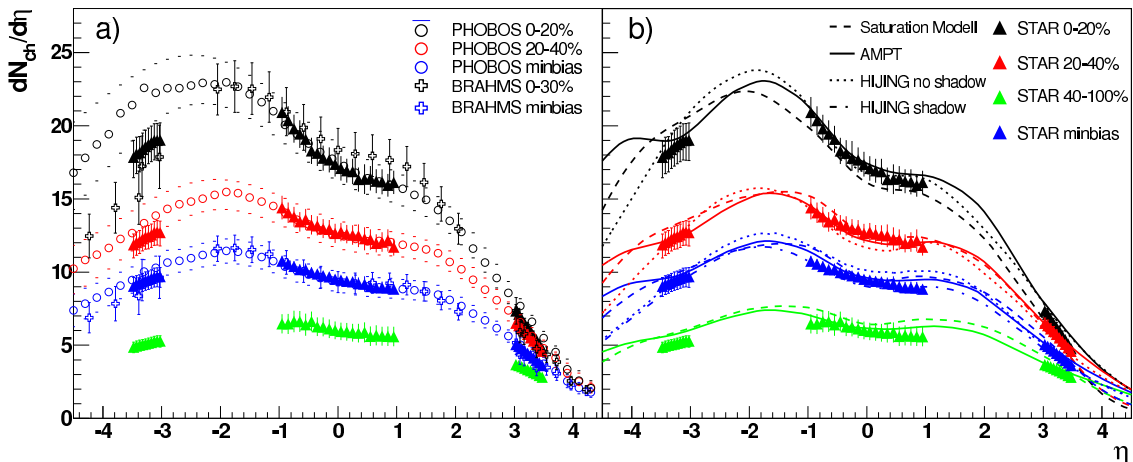


FIG. 3: (Color online) Charged hadron pseudorapidity distribution per event in the TPC and FTPC acceptance for 0-20%, 20-40%, 40-100% central and minimum bias d+Au events (triangles). The error bars include both statistical and systematic error. Also overlayed are measurements from BRAHMS (crosses) [22] and PHOBOS (circles) [23, 24]. In addition predictions from HIJING [19], AMPT [25] and the saturation model [12] are also plotted compared with STAR measurements.

which indicates that the Cronin effect is more pronounced on the Au-side of a d+Au collision. Strong centrality dependence of R_{CP} on the d-side of the collisions is another interesting feature seen in Fig. 2. This observation was also reported by the BRAHMS collaboration [11]. However, no significant centrality dependence is observed on the Au-side of a d+Au collision. The R_{CP} measurements from the FTPCs are in good overall agreement with measurements from BRAHMS on the d-side [11] for $p_t > 1$ GeV/c and in agreement with PHENIX on the Au-side [14] of a d+Au collision (see Fig. 2). The discrepancy between the BRAHMS and STAR R_{CP} measurements on the d-side at $\eta \approx 3$ for $p_t < 1$ GeV/c can not be completely resolved at this time. The discrepancy can be partially attributed to the different centrality classes used by the two experiments to calculate the R_{CP} . BRAHMS uses 60-80% as the most peripheral bin whereas STAR uses the 40-100% centrality class. Also, the BRAHMS centrality selection is biased towards peripheral collisions in forward rapidities as discussed in section III C. Furthermore, different low- p_t cut-offs may affect the low p_t measurements, where the difference between BRAHMS and STAR is most prominent.

The suppression of R_{CP} (and R_{dAu} [32]) at higher rapidities on the d-side is in qualitative agreement with predictions of the saturation model [12]. Models based on pQCD which incorporate initial-state parton scattering and energy loss can also describe the behaviour of R_{CP} at higher rapidities [8, 9]. Furthermore, in the framework of parton recombination in the final state, R_{CP} at forward rapidities can be described as well [13].

C. Charged particle density asymmetry

In Fig. 3a the pseudorapidity distribution $dN_{ch}/d\eta$ of charged hadrons per event in the TPC and FTPC acceptance is shown for minimum bias and for the 0-20%, 20-

40%, and 40-100% most central events. For comparison, measurements of the pseudorapidity distribution from BRAHMS [22] and PHOBOS [23, 24] are also plotted. The measured $dN_{ch}/d\eta$ distributions for minimum bias d+Au events are in good agreement for all three experiments. However, with increasing centrality, a significant difference in the particle density at negative pseudorapidity values $\eta < -3$ between STAR and PHOBOS is visible. On the other hand, the measurements in the mid-pseudorapidity region are in good agreement. When comparing central events, for the $\eta < -3$ region the BRAHMS $dN_{ch}/d\eta$ distribution is lower than the STAR measurements; at mid-rapidity it is higher. A possible explanation could be the different methods used for centrality selection. Centrality selection for the STAR-TPC was done via the N_{ch} multiplicity in the FTPC and vice versa, to avoid autocorrelations caused by fluctuations in the measured multiplicity. Simulation studies show that with a pseudorapidity gap of 2 units between the detectors this method is insensitive to autocorrelations [20]. Use of the FTPC N_{ch} multiplicity on the Au-side instead leads to a visibly higher particle density in the $dN_{ch}/d\eta$ distribution for $\eta < -3$, causing a significant bias in the centrality definition [20]. This observation explains the higher particle density measured by PHOBOS for the Au-side of a d+Au collision, because their centrality was determined via the multiplicity in the pseudorapidity region of $-4 < \eta < -3.5$. For BRAHMS the enhancement in the particle density at midrapidity could be due to the fact that the multiplicity in the central region $|\eta| < 2.2$ was used to define centrality. However, within the systematic errors the results of all three experiments are consistent with each other.

In addition, the measured pseudorapidity distributions were compared with model predictions. Calculations based on gluon saturation in the Color Glass Condensate [12] as well as results of HIJING [19] and a Multi-Phase Transport Model (AMPT) [26] are shown in Fig. 3b. All

model calculations are in good overall agreement with the measured $dN_{ch}/d\eta$ distributions for different centrality classes. In particular, the models are able to reproduce the increasing asymmetry of charged particle densities with increasing centrality.

IV. COLLISION ASYMMETRY AND YIELD SUPPRESSION

In the following section the centrality dependence of R_{CP} at high rapidities $|\eta| \approx 3.1$ will be discussed in connection with the observed increasing asymmetry of the produced particle density in d+Au collisions at transverse momenta $p_t < 3$ GeV/c. In Fig. 2, the R_{CP} from HIJING simulations for different centralities with and without shadowing is shown. It is evident from Fig. 2 that HIJING reproduces the overall behaviour of R_{CP} at $|\eta| \approx 3.1$. In addition, it can be concluded that the influence of shadowing for $p_t > 1$ GeV/c only affects the measurements on the Au-side. Since the p_t spectrum on the d-side is more or less independent of centrality – except for an overall scale – (see Fig. 1a and b) and comparable with p+p collisions, the suppression of R_{CP} on the d-side (see Fig. 2) could be due to the asymmetry in particle production in d+Au collisions with respect to the symmetric p+p collisions (see Fig. 4). To take the asymmetry in d+Au collisions into account, a new variable η_{CM} is introduced, which is defined as the weighted mean of the $dN_{ch}/d\eta$ distribution for each centrality class ($\eta_{CM} = \eta_{CM}(N_{part})$). η_{CM} was extracted from the published PHOBOS results [24] and should represent the shift of the center-of-mass in the asymmetric d+Au collisions with respect to the nucleon-nucleon center-of-mass system (see Table II). Even though the PHOBOS data are biased towards higher multiplicity on the Au-side as discussed in section III C they were used to determine η_{CM} to maintain a model independent approach (also they are the only measurements available covering the full η range). The $dN_{ch}/d\eta$ distribution for inelastic p+p collisions [22] in this new reference system - obtained by shifting with η_{CM} - are shown in Fig. 4. One observes that the d+Au $dN_{ch}/d\eta$ distributions normalized with $\langle N_{part}/2 \rangle$ (see Table I) at high rapidities are consistent with the shifted p+p values. Also, the centrality dependence can be qualitatively explained. Therefore, η_{CM} seems to be an appropriate variable to describe the asymmetry in particle production in d+Au collisions assuming that this asymmetry is caused by the nuclear stopping of the deuteron while traversing through the gold nucleus. Similar approaches to describe the pseudorapidity distributions in d+Au can be found in [20, 27, 28].

In that representation, the suppression of the particle density on the d-side and the enhancement on the Au-side in asymmetric d+Au collisions with respect to the symmetric p+p collisions (see Fig. 4) can be expressed by defining $S_{dAu}(\eta, \eta_{CM})$ as the ratio of the p+p reference $dN_{ch}^{pp}/d\eta$ distribution shifted with η_{CM}

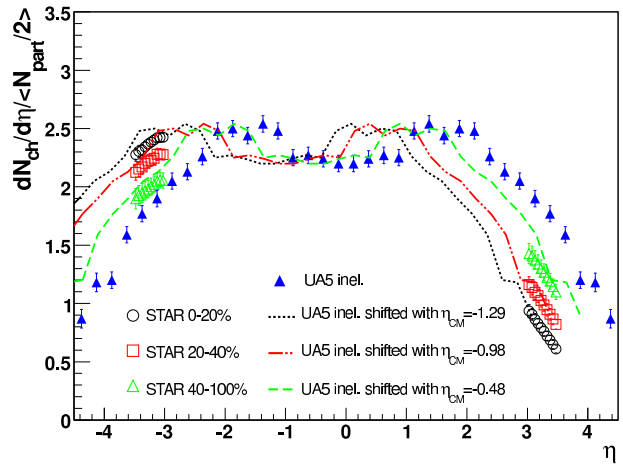


FIG. 4: (Color online) Pseudorapidity distribution of charged hadrons in the FTPC acceptance for 0-20%, 20-40%, 40-100% central d+Au events scaled with N_{part} (open triangles). p+p measurements [25] unshifted (triangles) and shifted by η_{CM} (lines) are overlaid (for further details see text).

Centrality class	η_{CM}
0-20%	-1.29
20-40%	-0.98
40-60%	-0.68
60-80%	-0.37
80-100%	-0.14
40-100%	-0.48
0-100%	-0.92

TABLE II: η_{CM} defined as the weighted mean of the PHOBOS $dN_{ch}/d\eta$ distribution for various centrality classes [24].

($dN_{ch}^{pp}/d\eta|_{\eta-\eta_{CM}}$) and the unshifted $dN_{ch}^{pp}/d\eta$ distribution:

$$S_{dAu}(\eta, \eta_{CM}) = \frac{dN_{ch}^{pp}/d\eta|_{\eta-\eta_{CM}}}{dN_{ch}^{pp}/d\eta|_{\eta}}(\eta, \eta_{CM}). \quad (2)$$

Our ansatz is then that the suppression and enhancement of R_{dAu} (and R_{CP}) is mainly caused by this geometric asymmetry. It would follow from this ansatz that the difference in the observed centrality dependence of R_{dAu} should be accounted for by simply scaling with $S_{dAu}(\eta, \eta_{CM})$ (Eq. 2). The BRAHMS R_{dAu} measurements [11] at different pseudorapidities ($\eta=0, 1, 2.2$ and 3.2) on the d-side are then consistent with a universal behaviour, reaching binary scaling at $p_t > 3$ GeV without a significant Cronin enhancement at intermediate p_t .

A similar procedure can be applied to describe R_{CP} measurements for different centrality classes and pseudorapidities on the d- and Au-side of a d+Au collision. One has to modify $S_{dAu}(\eta, \eta_{CM})$ (Eq. 2) to take the asymmetry in particle production - still visible in peripheral d+Au collisions (see Fig. 4) - into account. This is realized by taking the peripheral d+Au $dN_{ch}/d\eta$ distribution as reference and shifting the denominator in Eq. 2

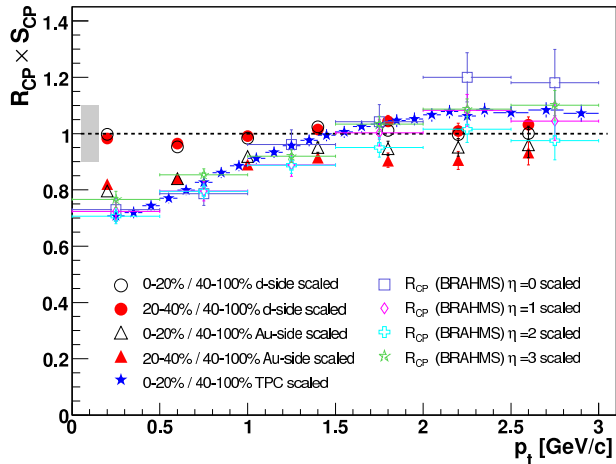


FIG. 5: (Color online) R_{CP} of charged hadrons at $\eta \approx -3.1$ (Au-side) and at $\eta \approx 3.1$ (d-side) as function of p_t for different centrality classes scaled with $S_{CP}(\eta, \eta_{CM})$ (Eq. 3). Midrapidity scaled charged hadron R_{CP} (0-20%) ($|\eta| < 0.5$) is shown as stars [21]. Also plotted are scaled BRAHMS R_{CP} measurements (0-20%/60-80%) [11] in different η intervals.

according to the peripheral η_{CM} value:

$$S_{CP}(\eta, \eta_{CM}) = \frac{dN_{ch}^{pp}/d\eta|_{\eta-\eta_{CM}}}{dN_{ch}^{pp}/d\eta|_{\eta-\eta_{CM,periph}}}(\eta, \eta_{CM}). \quad (3)$$

R_{CP} measurements from the FTPCs at $|\eta| \approx 3.1$ for different centrality classes scaled with $S_{CP}(\eta, \eta_{CM})$ are shown in Fig. 5. These results suggest that the observed enhancement of R_{CP} on the Au-side for different centrality classes can be explained by an enhancement of particle production caused by the nuclear stopping of the deuteron and described by a shift of the center-of-mass with respect to the most peripheral d+Au collisions. The suppression of R_{CP} on the d-side is explained analogously. Universal scaling behaviour of R_{CP} scaled with $S_{CP}(\eta, \eta_{CM})$ at $|\eta| \approx 3.1$ is visible for $p_t > 1$ GeV/c in the FTPC measurements (see Fig. 5). In addition scaled BRAHMS R_{CP} measurements for the top 20% central d+Au events at different pseudorapidities are also overlaid in Fig. 5. Universal scaling behaviour of scaled R_{CP} is seen in both STAR and BRAHMS measurements reaching binary scaling for $p_t > 2$ GeV/c. The deviation from the supposed scaling for the BRAHMS R_{CP} measurements at midrapidity (and also the discrepancy to the STAR midrapidity measurements) might be explained by the different centrality definitions, where a bias to higher particle multiplicities might be present in the BRAHMS data as discussed in section III C. It should be noted that systematic errors in the scaling due to uncertainties in the determination of η_{CM} were not estimated in this analysis. One would expect an overall normalization uncertainty, but the main feature of scaling should be preserved. The simple data driven picture outlined in this paper was meant to point out the importance of the collision geometry in d+Au collisions.

V. CONCLUSIONS

Centrality dependence of the $dN/d\eta$ distributions in $\sqrt{s_{NN}}=200$ GeV d+Au collisions is presented. Within errors, $dN/d\eta$ cannot discriminate between different model calculations. However, our data show an increase of $\langle p_t \rangle$ as a function of centrality on the Au-side, whereas on the d-side no centrality dependence is visible. This result together with the suppression of R_{CP} on the d-side and its enhancement on the Au-side relative to mid-rapidity cannot be described consistently by current model calculations [15]. A similar study of comparing particle production at high p_t in d- and Au-side at mid-rapidity [29] has ruled out models based on incoherent initial multiple partonic scattering and independent fragmentation. It also showed that models based on nuclear shadowing incorporating extremes of gluon shadowing at low x can not account for the difference in particle production in d- and Au-side at high p_t at mid-rapidity.

This paper demonstrated, that in a simple stopping picture the main features of the pseudorapidity and centrality dependence of R_{CP} (and R_{dAu}) at higher rapidities can be explained by the suppression (enhancement) of particle yields in d+Au relative to p+p collisions and peripheral d+Au collisions. Simulation studies show a small effect of shadowing in HIJING on R_{CP} , especially on the d-side, supporting this geometric picture. This result is also confirmed by measurements of R_{pPb} by NA49 [30] at an order of magnitude lower energies, where shadowing and gluon saturation are expected to be small, which show qualitatively the same characteristic centrality and rapidity (x_F) dependence and are consistent with the stopping picture.

Taking the asymmetry in particle production – characterized by a shift of the center-of-mass in the asymmetric d+Au collisions with respect to the nucleon-nucleon or peripheral d+Au center-of-mass system – into account, R_{CP} (and R_{dAu}) show a universal scaling behaviour independent of centrality and pseudorapidity in d+Au collisions at RHIC energies. On the other hand, the success of the CGC saturation approach [31] and stopping picture in quantitatively describing BRAHMS R_{CP} (and R_{dAu}) measurements could be interpreted as a link between saturation as the possible origin of nuclear stopping. In that case deviations from the observed empirical scaling in asymmetric collision systems at different energies can help to quantify the onset of saturation effects in heavy-ion collisions.

We thank the RHIC Operations Group and RCF at BNL, and the NERSC Center at LBNL for their support. This work was supported in part by the HENP Divisions of the Office of Science of the U.S. DOE; the U.S. NSF; the BMBF of Germany; IN2P3, RA, RPL, and EMN of France; EPSRC of the United Kingdom; FAPESP of Brazil; the Russian Ministry of Science and Technology; the Ministry of Education and the NNSFC of China; IRP and GA of the Czech Republic,

FOM of the Netherlands, DAE, DST, and CSIR of the Government of India; Swiss NSF; the Polish State Committee for Scientific Research; STAA of Slovakia,

and the Korea Sci. & Eng. Foundation.

-
- [1] C. Adler et al. (STAR), Phys. Rev. Lett. **90**, 082302 (2003), nucl-ex/0210033.
- [2] D. Kharzeev, E. Levin, and L. McLerran, Phys. Lett. B **561**, 93 (2003).
- [3] J. Adams et al. (STAR), Phys. Rev. Lett. **91**, 072304 (2003), nucl-ex/0306024.
- [4] B. B. Back et al. (PHOBOS), Phys. Rev. Lett. **91**, 072302 (2003), nucl-ex/0306025.
- [5] S. S. Adler et al. (PHENIX), Phys. Rev. Lett. **91**, 072303 (2003), nucl-ex/0306021.
- [6] I. Arsene et al. (BRAHMS), Phys. Rev. Lett. **91**, 072305 (2003), nucl-ex/0307003.
- [7] J. W. Cronin et al., Phys. Rev. D **11**, 3105 (1975).
- [8] I. Vitev, Phys. Lett. B **562**, 36 (2003).
- [9] X.-N. Wang, Phys. Lett. B **565**, 116 (2003), nucl-th/0303004.
- [10] D. Kharzeev and E. Levin, Phys. Lett. B **523**, 79 (2001), nucl-th/0108006.
- [11] I. Arsene et al. (BRAHMS), Phys. Rev. Lett. **93**, 242303 (2004), nucl-ex/0403005.
- [12] D. Kharzeev, E. Levin, and M. Nardi, Nucl. Phys. A **730**, 448 (2004), hep-ph/0212316.
- [13] R. C. Hwa, C. B. Yang, and R. J. Fries, Phys. Rev. C **71**, 024902 (2005), nucl-th/0410111.
- [14] S. S. Adler et al. (PHENIX), Phys. Rev. Lett. **94**, 082302 (2005), nucl-ex/0411054.
- [15] A. Accardi, Acta Phys. Hung. **A22**, 289 (2005), nucl-th/0405046.
- [16] K. H. Ackermann et al. (STAR), Nucl. Inst. Meth. A **499**, 624 (2003).
- [17] M. Anderson et al. (STAR), Nucl. Inst. Meth. A **499**, 659 (2003).
- [18] K. H. Ackermann et al. (STAR), Nucl. Inst. Meth. A **499**, 713 (2003).
- [19] X.-N. Wang and M. Gyulassy, Phys. Rev. D **44**, 3501 (1991).
- [20] J. Putschke, Ph.D. thesis, Max-Planck-Institut für Physik, München (2004).
- [21] J. Adams et al. (STAR), Phys. Rev. C **70**, 064907 (2004).
- [22] I. Arsene et al. (BRAHMS), Phys. Rev. Lett. **94**, 032301 (2005), nucl-ex/0401025.
- [23] B. B. Back et al. (PHOBOS), Phys. Rev. Lett. **93**, 082301 (2004), nucl-ex/0311009.
- [24] B. B. Back et al. (PHOBOS), Phys. Rev. C **72**, 031901 (2005), nucl-ex/0409021.
- [25] G. J. Alner et al. (UA5), Z. Phys. C **33**, 1 (1986).
- [26] Z.-w. Lin and C. M. Ko, Phys. Rev. C **68**, 054904 (2003), nucl-th/0301025.
- [27] J. Putschke (STAR), J. Phys. Conf. Ser. **5**, 37 (2005).
- [28] P. Steinberg (2007), nucl-ex/0703002.
- [29] B. I. Abelev (STAR) (2006), nucl-ex/0609021.
- [30] B. Boimska, Ph.D. thesis, Institute for Nuclear Studies, Warsaw (2004).
- [31] D. Kharzeev, Y. V. Kovchegov, and K. Tuchin, Phys. Lett. **B599**, 23 (2004), hep-ph/0405045.
- [32] $R_{AB}(p_t) = (d^2N/dp_t d\eta)/(T_{AB}d^2\sigma^{pp}/dp_t d\eta)$, where $d^2N/dp_t d\eta$ is the differential yield per event in the nuclear collision A+B and $T_{AB} = \langle N_{bin} \rangle / \sigma_{inel}^{pp}$ describes the nuclear geometry with respect to the p+p reference measurements.